Tau protein is essential for stress-induced brain pathology

Sofia Lopes[a,b], João Vaz-Silva[a,b], Vitor Pinto[a,b], Christina Dalla[c], Nikolaos Kokras[c], Benedikt Bedenk[d], Natalie Mack[d], Michael Czisch[d], Osborne F. X. Almeida[d], Nuno Sousa[a,b], and Ioannis Sotiropoulos[a,b,1]

[a]Life and Health Sciences Research Institute (ICVS), School of Health Sciences, University of Minho, 4710-057 Braga, Portugal; [b]ICVS/3B's-PT Government Associate Laboratory, 4710-057 Braga/Guimarães, Portugal; [c]Department of Pharmacology, Medical School of Athens, 11527 Goudi, Greece; and [d]Max Planck Institute of Psychiatry, 80804 Munich, Germany

Edited by Bruce S. McEwen, The Rockefeller University, New York, NY, and approved May 2, 2016 (received for review January 28, 2016)

Exposure to chronic stress is frequently accompanied by cognitive and affective disorders in association with neurostructural adaptations. Chronic stress was previously shown to trigger Alzheimer's-like neuropathology, which is characterized by Tau hyperphosphorylation and missorting into dendritic spines followed by memory deficits. Here, we demonstrate that stress-driven hippocampal deficits in wild-type mice are accompanied by synaptic missorting of Tau and enhanced Fyn/GluN2B-driven synaptic signaling. In contrast, mice lacking Tau [Tau knockout (Tau-KO) mice] do not exhibit stress-induced pathological behaviors and atrophy of hippocampal dendrites or deficits of hippocampal connectivity. These findings implicate Tau as an essential mediator of the adverse effects of stress on brain structure and function.

Tau | stress | hippocampus | depression | memory deficits

The cytoskeletal protein Tau is implicated in the establishment of Alzheimer's disease (AD) (1) as well as excitotoxicity (1) and, more recently, epilepsy (2, 3). Exposure to stressful conditions induces depressive behavior and memory deficits in both rodents and humans (4–8). Studies in rodents have shown that chronic stress triggers Tau hyperphosphorylation, a key pathogenic mechanism in AD, and results in cognitive and mood deficits (9–13); however, those studies do not provide direct evidence for a role of Tau in stress-evoked brain pathology. Given that Tau plays an important role in regulating neuronal architecture and function through its interaction with various cellular targets (e.g., tubulin and Fyn) (14), we hypothesized that Tau mediates the deleterious actions of stress on brain structure and function.

To test the above hypothesis, we compared the impact of chronic unpredictable stress (CUS) (11, 15) in mice carrying a null mutation of the *mapt* gene [Tau knockout (Tau-KO) mice] (16) with their wild-type (WT) littermates. Three well-characterized behavioral endpoints (cognition, coping styles, and anxiety) that are disrupted by CUS served as the primary assay endpoints; these were complemented with measures of hippocampal structural and functional integrity. The hippocampus is a central component of the neurocircuitries that control these behaviors and displays overt lesions in both stress- and Tau-related pathologies; in the latter, the hippocampus is one of the earliest brain regions to show signs of neurodegeneration (1, 4, 7, 10–13, 17).

Results

Deleterious Effects of Stress on Memory and Mood Are Abrogated in the Absence of Tau Protein. Cognition, mood, and anxiety are interdependent behavioral domains that exhibit complex interactions (5). Different forms of memory were assessed after exposure of WT and Tau-KO mice to the CUS paradigm; the test battery included the Y-maze, Morris water maze (MWM), and the novel object recognition test (NOR). Anxiety was evaluated using the elevated plus maze (EPM), and coping styles and anhedonia were assessed using the forced swim test (FST) and the sucrose consumption test (SCT).

Two-way ANOVA analysis of the Y-maze data revealed CUS × Genotype interactions for both, distance traveled [$F_{(1, 65)} = 4.024$, $P = 0.04$], and time spent [$F_{(1, 65)} = 4.614$, $P = 0.03$] in the novel arm of the apparatus. Exposure to CUS resulted in deficits in spatial memory in WT ($p_{dist} = 0.02$; $p_{time} = 0.02$), but not Tau-KO ($p_{dist} = 0.98$; $p_{time} = 0.95$), mice; no differences were found between WT and Tau-KO control (nonstressed) animals ($p_{dist} = 0.84$; $p_{time} = 0.77$) (Fig. 1*A* and *SI Appendix*, Fig. S1). Total distance traveled in the three arms of the maze did not differ between any of the groups (Fig. 1*B*). Results from the MWM test confirmed that CUS induces impairments in spatial learning/memory in WT, but not Tau-KO, mice [significant CUS × Genotype interaction in distance swum to reach the escape platform [$F_{(1, 35)} = 7.467$, $P = 0.01$]; CUS increased the distance swum in WT mice only ($P \leq 0.05$) (Fig. 1*C*). The NOR test showed that recognition memory was also disrupted by CUS in WT, but not Tau-KO, mice. Specifically, we found a CUS × Genotype interaction [$F_{(1, 37)} = 4.387$, $P = 0.04$] on the discrimination index. Importantly, this index was reduced by CUS in WT ($p_{WT} = 0.01$), but not Tau-KO ($p_{KO} = 0.83$), mice; control WT and Tau-KO mice did not differ on this parameter ($P = 0.60$) (Fig. 1*D*).

Testing in the EPM (Fig. 1*E*) showed that CUS elicits an anxiogenic phenotype in WT, but not Tau-KO, animals [two-way ANOVA, CUS × Genotype interaction: $F_{(1, 84)} = 4.004$, $P = 0.04$; overall effect of CUS ($F_{(1, 84)} = 6.296$, $P = 0.01$)] with WT animals spending significantly less time in the open arms of the maze ($p_{WT} = 0.01$ vs. $p_{KO} = 0.98$). Furthermore, we used two different tests to monitor active or passive coping styles (18) and anhedonic behavior. FST revealed a CUS × Genotype interaction [$F_{(1, 73)} = 4.071$, $P = 0.04$] and an overall effect of CUS [$F_{(1, 73)} = 6.229$, $P = 0.01$] on time of immobility (passive

Significance

Exposure to stressful events is a well-known inducer of neuronal atrophy implicated in the development of neuropsychiatric and neurological pathologies (e.g., depression and Alzheimer's disease), although the underlying molecular mechanisms remain elusive. The current study demonstrates that absence of the cytoskeletal protein Tau blocks stress-evoked hippocampal synaptic signaling and morphofunctional damages related to both neuronal structure and connectivity as well as subsequent behavioral deficits. These findings suggest, for the first time to our knowledge, that Tau protein is a key regulator of neuronal malfunction found in stress-driven hippocampal pathology.

Author contributions: N.S. and I.S. designed research; S.L., J.V.-S., V.P., C.D., N.K., B.B., N.M., M.C., and I.S. performed research; O.F.X.A., N.S., and I.S. contributed new reagents/analytic tools; S.L., J.V.-S., V.P., C.D., N.K., B.B., N.M., M.C., O.F.X.A., N.S., and I.S. analyzed data; and O.F.X.A., N.S., and I.S. wrote the paper.

The authors declare no conflict of interest.

This article is a PNAS Direct Submission.

[1]To whom correspondence should be addressed. Email: ioannis@ecsaude.uminho.pt.

This article contains supporting information online at www.pnas.org/lookup/suppl/doi:10.1073/pnas.1600953113/-/DCSupplemental.

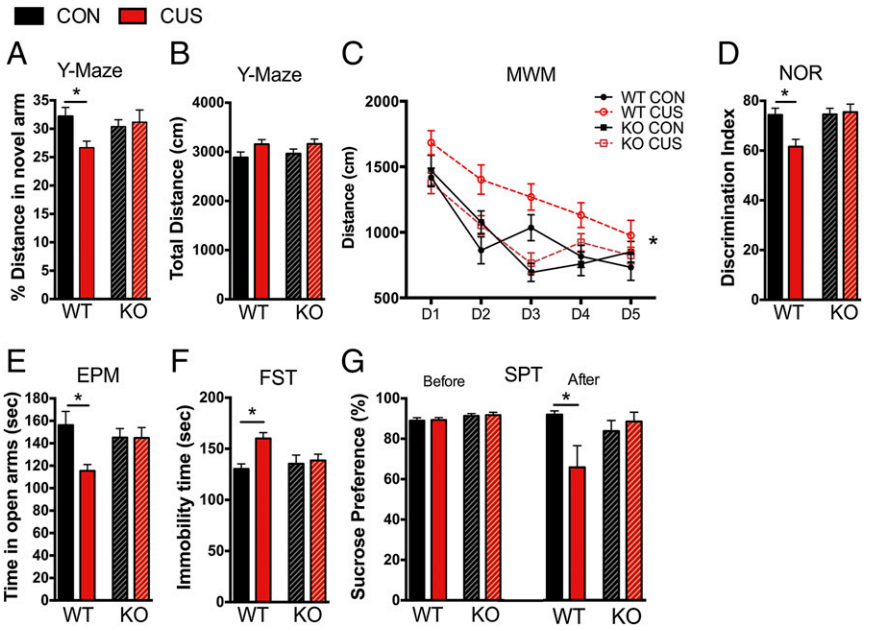

Fig. 1. Tau ablation blocks stress-driven anxious, anhedonic, and passive coping behaviors as well as cognitive impairments. (*A* and *B*) Chronic unpredictable stress (CUS) decreased the distance traveled by WT animals traveled in the novel arm of the Y-maze apparatus, indicating a deficit in spatial memory (*SI Appendix*, Fig. S1); this deficit was not displayed by CUS-exposed Tau-KO animals. Note that both WT and Tau-KO covered similar distances in the maze. (*C*) The Morris water maze (MWM) test revealed impairments of spatial learning/memory in WT, but not Tau-KO, animals that had been exposed to CUS as CUS-WT animals traveled greater distances to reach the escape platform vs. control WT mice. (*D*) In contrast to Tau-KOs, WT animals displayed decreased discrimination index after CUS exposure when tested in the novel object recognition (NOR) test; this suggests CUS-evoked impaired recognition memory in WT animals. (*E*) Exposure to CUS produced higher levels of anxiety in WT, but not Tau-KO, mice, as seen by the reduced time spent in the open arms of the elevated plus maze (EPM) in WT animals. (*F*) WT animals exposed to CUS exhibited increased immobility time in the forced swim test (FST), reflecting passive coping behavior compared with WT controls (CON); no difference between CUS and CON Tau-KOs was found. (*G*) Reduced preference for the sucrose solution (which reflects anhedonic behavior) was observed in CUS-exposed WT, but not Tau-KO, mice in the sucrose preference test (SPT), indicating their sensitivity to the effects of CUS. Note that all treatment groups showed a similar preference for sucrose before the CUS paradigm. All data shown represent mean ± SEM (*$P < 0.05$).

behavior). Furthermore, CUS-treated WT mice displayed longer periods of immobility ($P = 0.01$) than Tau-KO ($P = 0.98$) mice, compared with their respective non-CUS-treated (control) counterparts (Fig. 1*F*); these findings were confirmed by measuring latency to immobility (*SI Appendix*, Fig. S2). Results from the SCT, which provides an index of anhedonia or appetite (a cardinal symptom of depression in humans), showed a significant CUS × Genotype interaction [$F_{(1, 30)} = 5.906$, $P = 0.02$], with post hoc analysis revealing reduced sucrose consumption in WT ($P = 0.03$), but not Tau-KO ($P = 0.94$), mice (Fig. 1*G*, *Right*). The above sets of data demonstrate that Tau-KO mice are resistant to the behavioral effects of stress on memory, coping styles, and anxiety.

Tau Deletion Does Not Interfere with the Endocrine Response to Stress. The ability of chronic stress to interfere with cognitive and affective functions is largely attributable to the actions of glucocorticoids [e.g., corticosterone (CORT) in rodents], which are released in response to stress (6). In contrast to the genotype-specific behavioral responses to CUS, both WT and Tau-KO mice displayed similar elevations in blood CORT and body mass loss following the CUS paradigm (*SI Appendix*, Table S1) and responded to an acute stressor (4-min restraint) with similar increases in CORT secretion (*SI Appendix*, Table S2). These observations suggest that the above Tau-dependent detrimental effects of stress on behavior are not due to differential regulation of the endocrine response to stress in WT and Tau-KO animals.

Tau Ablation Attenuates Stress-Induced Disruption of Neuronal Connectivity. Reductions in monoaminergic tone, specifically of noradrenaline (NA) and serotonin (5-HT), play a central role in mediating the detrimental effects of stress on cognition and mood (19). Consistent with the failure of CUS to cause behavioral changes in Tau-KO mice, NA and 5-HT levels in the hippocampus were found to be altered in WT, but not in Tau-KO, mice (Fig. 2). Specifically, we detected significant Genotype × CUS interactions [$F_{(1, 16)}$ NA = 7.639, $P = 0.01$; $F_{(1, 16)}$ 5-HT = 6.954, $P = 0.02$], and post hoc analysis revealed significant CUS-induced reductions in hippocampal monoamine levels in WT (NA: $P = 0.02$; 5-HT: $P = 0.04$) vs. no changes in Tau-KO (NA: $P = 0.96$; 5-HT: $P = 0.97$) animals (Fig. 2 *A* and *B*). Genotype did not influence the effect of CUS on NA and 5-HT levels (NA: $P = 0.95$; 5-HT: $P = 0.97$). Calculations of 5-HT turnover ratio from parallel measurement of the 5-HT metabolite, 5-hydroxyindole acetic acid (5-HIAA), confirmed that CUS altered 5-HT turnover in WT ($P = 0.04$), but not Tau-KO ($P = 0.99$), animals, indicated by an interaction effect between CUS and Genotype [$F_{(1, 16)} = 4.628$, $P = 0.04$] (*SI Appendix*, Fig. S3). Examining hippocampal levels and turnover of dopamine (DA) did not reveal any significant effect of CUS in either WT or Tau-KO mice (Fig. 2*A* and *SI Appendix*, Fig. S3).

We next monitored the impact of stress on hippocampal synaptic plasticity by measuring the inducibility of long-term potentiation (LTP) in slice preparations (Fig. 2 *C* and *D*) (20). Analysis of the LTP data revealed a significant CUS × Genotype interaction [$F_{(1, 27)} = 6.283$, $P = 0.018$] and overall effects of CUS [$F_{(1, 27)} = 11.24$, $P = 0.002$] and Genotype [$F_{(1, 27)} = 41.35$, $P < 0.0001$]. In addition, post hoc analysis revealed that LTP was reduced in slices from CUS-treated WT ($P = 0.002$), but not CUS-treated Tau-KO ($P = 0.92$), mice compared with their controls. Interestingly, LTP levels differed between WT and Tau-KO animals ($P < 0.0001$). These changes were accompanied by altered synaptic release probability, as assessed by monitoring paired-pulse (PP) facilitation at different interstimulus intervals (Fig. 2 *E* and *F*) (17): PP ratios (25 and 50 ms interpulse intervals)

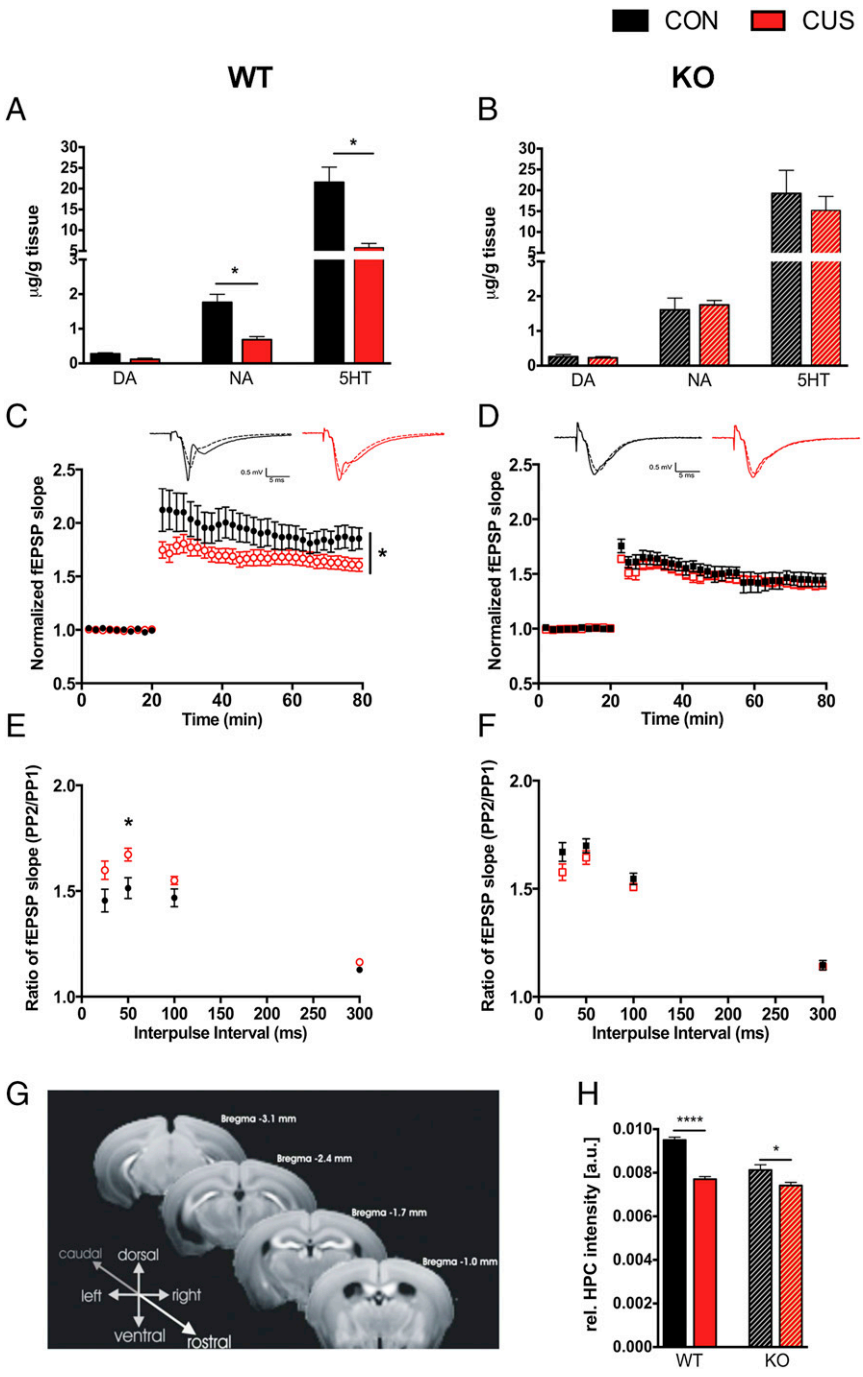

Fig. 2. Hippocampal function and activity is differentially affected by stress in WT and Tau-KO animals. (*A* and *B*) Monoamine [dopamine (DA), noradrenaline (NA), and serotonin (5HT)] levels in the hippocampi of control and CUS-treated WT (*A*) and Tau-KO (*B*) mice are shown. CUS decreased NA and 5HT levels in WT, but not Tau-KO, animals. Metabolites and turnover rates of these monoamines in the various treatment groups are depicted in *SI Appendix*, Fig. S3. (*C* and *D*) LTP, induced by 100 Hz stimulation, was significantly diminished in WT-CUS animals compared with WT CON. LTP was not altered by CUS exposure in Tau-KO animals. (*E* and *F*) Paired-pulse facilitation was increased by CUS in WT, but not Tau-KO, animals, indicating reduced release probability in the former group. (*G*) MEMRI coronal images show strong contrast enhancement in the hippocampus reflecting activity-dependent Manganese accumulation. (*H*) MEMRI analysis revealed that CUS reduces hippocampal neuronal activity in both WT and Tau-KO mice, but to a significantly greater extent in WT-CUS animals. All data shown represent mean ± SEM (*$P < 0.05$; ****$P < 0.0001$).

were subject to CUS × Genotype interactions [$F_{(1,\ 27)}$ 25 ms = 7.100, $P = 0.012$; $F_{(1,\ 27)}$ 50 ms = 9.148, $P = 0.005$], and Genotype had an overall effect on this parameter [$F_{(1,\ 27)}$ 25 ms = 4.777, $P = 0.037$; $F_{(1,\ 27)}$ 50 ms = 5.034, $P = 0.033$]. Post hoc analysis revealed that CUS decreases the probability of synaptic release in slices of WT ($p_{50ms} = 0.02$), but not Tau-KO ($p_{50ms} = 0.66$), mice (Fig. 2 *E* and *F*). Interestingly, basal synaptic transmission, assessed using input–output curves, did not differ between any of the groups tested (*SI Appendix*, Fig. S4).

Next, we compared the effects of CUS on hippocampal neuronal activity using manganese (Mn)-enhanced magnetic resonance imaging (MEMRI) (21) to detect hippocampal neuronal activity;

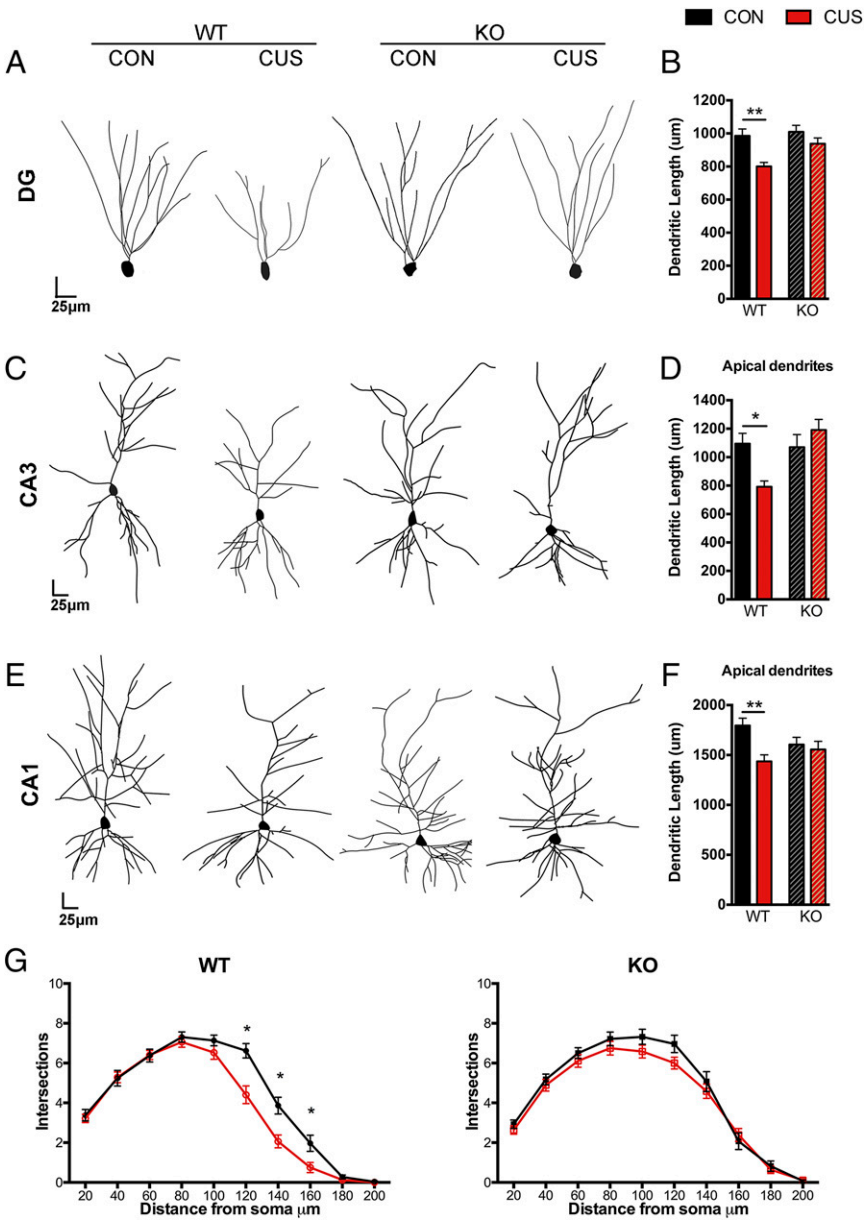

Fig. 3. Stress-driven structural remodeling of hippocampal neurons depends on Tau protein. (*A–F*) Golgi-impregnated hippocampal sections were used to examine the effects of CUS on neuronal atrophy and dendritic lengths. Exposure to chronic stress (CUS) resulted in neuronal atrophy in the dentate gyrus, CA3 and CA1 subfields of WT animals, as shown by 3D neuronal reconstruction (*A*, *C*, and *E*) and morphometry (*B*, *D*, and *F*). In contrast, Tau-KO mice did not show any atrophy after exposure to CUS. (*G*) CUS was found to lead to a reduction in dendritic arborization of DG neurons in WT-CUS vs. CON-WT mice, whereas this parameter was not altered in CUS-treated Tau-KO mice (*SI Appendix*, Fig. S5). All numeric data represent mean ± SEM (*$P < 0.05$; **$P < 0.01$).

the method allows evaluation of local neural activity because Mn enters into neurons through calcium channels (21). Hippocampal MEMRI intensity was normalized to a nonbrain region (masseter muscle) (22). Data analysis showed a significant CUS × Genotype interaction [two-way ANOVA $F_{(1,\ 44)} = 10.64$, $P = 0.0021$], an overall CUS [$F_{(1,\ 44)} = 25.00$, $P < 0.0001$], and a Genotype effect [$F_{(1,\ 44)} = 56.63$, $P < 0.0001$] (Fig. 2 *G* and *H*); it should be noted that the CUS × Genotype interaction resulted from the stronger CUS-induced reduction in neuronal activity in WT ($P < 0.001$) vs. Tau-KO ($P = 0.02$) mice. Finally, a significant difference of hippocampal neuronal activity was found between nonstressed WT and Tau-KO mice ($P < 0.001$).

Neuronal Atrophy in Stressed Hippocampus Is Tau-Dependent. Chronic stress exerts profound effects on neuronal architecture in the hippocampal formation, in particular on dendritic arborization in the dentate gyrus, CA1 and CA3 neurons (4, 6–8); these structural changes correlate with CUS-induced emotional and cognitive impairments (4, 7, 23). Examination of dendritic lengths in the various subfields of the rostral hippocampus by 3D reconstruction analysis of Golgi-stained tissues showed significant CUS × Genotype effects on the dendritic lengths of dentate granule [$F_{(1,\ 117)} = 3.944$, $P = 0.04$], CA1 (specifically, apical dendrites) [$F_{(1,\ 94)} = 4.440$, $P = 0.03$], and CA3 pyramidal [$F_{(1,\ 75)} = 8.481$, $P = 0.004$] neurons. Overall effects of CUS were found on dendritic lengths in the dentate [$F_{(1,\ 117)} = 11.310$, $P = 0.001$] and CA1 [$F_{(1,\ 94)} = 7.704$, $P = 0.006$] subfields, and Genotype influenced dentate [$F_{(1,\ 117} = 7.109$, $P = 0.008$] and CA3 [$F_{(1,\ 75)} = 6.641$, $P = 0.01$] neuron dendritic lengths. Post hoc analysis revealed that CUS significantly reduced dendritic lengths of hippocampal neurons in WT ($p_{DG} = 0.001$;

$p_{CA3} = 0.02$; $p_{CA1} = 0.005$), but not Tau-KO ($p_{DG} = 0.75$; $p_{CA3} = 0.62$; $p_{CA1} = 0.96$), mice (Fig. 3 *A–F*). No differences in apical dendritic length were found between control WT and Tau-KO animals ($p_{DG} = 0.96$, $p_{CA3} = 0.99$, $p_{CA1} = 0.27$). Consistent with previous findings, CUS did not influence the structure of the basal dendrites of CA1 and CA3 pyramidal cells (23). These alterations in dendritic atrophy were complemented by the results of Scholl analyses that showed that CUS reduces dendritic arborization in the hippocampus of WT, but not of Tau-KO, animals (Fig. 3*G* and *SI Appendix*, Fig. S5).

Chronic Stress Evokes Tau Hyperphosphorylation and Missorting in Synapses. Tau hyperphosphorylation and missorting in dendrites and synapses are considered key mechanisms in the neuronal damage and atrophy that characterize AD (24–27). In light of the above evidence that Tau is required for the manifestation of CUS-induced neuronal atrophy and dysfunction (Figs. 2 and 3), we next monitored the impact of CUS on Tau and its phosphorylation status in cytosolic and synaptosomal fractions from the hippocampi of WT mice (Fig. 4 *A–C*). CUS induced a significant increase in cytosolic levels of total Tau (*t* test, $P = 0.03$), accompanied by increased levels of Thr231-, Ser262-, and Ser396/404-Tau phospho-epitopes ($p_{231} = 0.03$; $p_{262} = 0.0001$; $p_{396/404} = 0.018$, respectively; Fig. 4 *D* and *E*); these findings indicate cytoplasmic accumulation of Tau. Although Tau is found mainly in the neuronal axon and soma, previous work suggests that Tau is missorted and accumulated at synapses under pathological conditions (24, 28). We show here that CUS elevates total Tau levels ($P = 0.02$) as well the levels of pSer262-Tau and pSer396/404-Tau isoforms ($P = 0.04$, $P = 0.03$, respectively) in synaptosomal fractions from WT hippocampi, indicating synaptic accumulation of these phospho-Tau forms (Fig. 4 *D* and *E*). Because the effects of chronic stress on neuronal structure and function are largely attributed to glucocorticoids (GC) (6, 7) and previous work from our team and others points toward the role of the glucocorticoid receptor (GR) in Tau hyperphosphorylation (10, 11), we next examined whether the actions of CUS could be reproduced by chronic administration of a potent synthetic GR agonist (dexamethasone). Immunoblotting analysis of fractionated hippocampal tissue (Fig. 4*A*) showed that GC treatment increases both cytosolic and synaptosomal levels of total Tau, as well as of phosphorylated Tau (*SI Appendix*, Fig. S6). These findings were substantiated by transmission electron microscopy (TEM) analysis of immunogold Tau-stained hippocampal sections (Fig. 4 *G* and *H* and *SI Appendix*, Fig. S7). This analysis demonstrated that GC exposure elevates the density of total Tau staining in dendrites and synapses ($P = 0.0002$ and $P = 0.0001$, respectively). Together, the above biochemical and TEM results suggest that CUS and GC lead to cytoplasmic accumulation of Tau as well as its missorting to hippocampal synapses, possibly leading to disturbed synaptic function, as recently suggested (24, 28).

Tau was recently found to participate in synaptic signaling by interacting with Fyn (29), a Src family kinase, that selectively modulates the function of the GluN2B-containing NMDA receptors (NMDARs) by phosphorylating the Y1472 residue of the GluN2B subunit (30). Synaptic missorting of Tau has been suggested to underpin synaptic toxicity by enhancing the postsynaptic targeting of Fyn (24), subsequently linking NMDARs to downstream synaptic excitotoxic signaling (24, 30). We show here that exposure to CUS increases levels of Fyn in postsynaptic density (PSD) fractions obtained from the hippocampi of WT ($P = 0.02$), but not Tau-KO ($P = 0.95$), mice [$F_{(1, 51)} = 5.94$, $P = 0.01$; Fig. 4 *I–K*]. Moreover, in line with previous reports (24), we found that Tau-KO animals express lower levels of PSD-associated Fyn [$F_{(1, 51)} = 17.2$, $P = 0.0001$]. Furthermore, we show that only WT mice respond to CUS with higher PSD levels of Y1472-phosphorylated GluN2B [$P = 0.01$; $F_{(1, 50)} = 4.10$, $P = 0.04$] and elevated levels of total GluN2B receptors in the PSD ($P = 0.03$; Fig. 4 *J* and *K*). Briefly, these observations are consistent with the view that Tau plays an essential mediatory role in Y1472 phosphorylation of GluN2B, an event that helps stabilize GluN2B receptors within the PSD enhancing its synaptic localization (24), whereas the absence of Tau attenuates the above stress-driven signaling.

In summary, the neurochemical, electrophysiological, molecular, and neuroanatomical evidence reported in this section demonstrates that CUS differentially influences the structural and functional integrity of the hippocampus in WT and Tau-KO mice; the latter "escape" stress-induced disruption of the hippocampal circuitry (cf. 7).

Discussion

The experiments reported here demonstrate that Tau protein is a critical mediator of the neuronal dysfunction and associated cognitive and affective impairments seen after the experience of chronic stress; they introduce a Tau-dependent cellular mechanism to explain the well-known causal relationship between stress and hippocampal malfunction (4, 6).

Clinical and preclinical studies have shown that prolonged exposure to stressful conditions impairs structural and functional plasticity of the hippocampal formation related to stress-driven cognitive and mood deficits (7, 8, 23). A key finding of this animal study is that Tau is essential for chronic stress to induce dendritic atrophy and interrupt neuronal connectivity in the hippocampus. Consistent with these structural and functional observations, animals lacking Tau were spared from the deleterious behavioral effects of chronic stress. Although our knowledge about the cellular mechanisms through which stress induces structural and functional remodeling of the hippocampus is limited, we previously showed that chronic stress increases the levels of two kinases (GSK3β and cdk5) that play a key role in the generation of aberrantly hyperphosphorylated Tau (11, 31). We now show that chronic stress leads to an accumulation of Tau and different isoforms of hyperphosphorylated Tau in the cytosolic and synaptic compartments of hippocampal neurons. Notably, phosphorylation in two epitopes of Tau, Thr231 and Ser262, is known to reduce the microtubule-binding capacity of Tau, which subsequently results in destabilization of the neuronal cytoskeleton, disrupted intracellular trafficking, and hippocampal atrophy in AD (26, 32–35). Recent evidence demonstrated that the intracellular distribution of Tau depends critically on the phosphorylation status of the protein (36). Accordingly, hyperphosphorylation of Tau seems to be necessary for missorting of Tau at synapses as only pseudophosphorylated Tau (which mimics hyperphosphorylated Tau), but not phosphorylation-deficient Tau, is mislocalized and accumulated in dendritic spines (25). Importantly, while amyloid β is a well-known trigger of Tau missorting and dendritic collapse (28, 37), our current findings represent the first demonstration, to our knowledge, that an exogenous stimulus—chronic stress—can also induce Tau missorting; they add to our mechanistic understanding of the impact of stressful conditions on the development of nonfamilial forms of AD, as previously suggested (38).

Tau missorting at dendritic spines is suggested to represent an early event in AD, preceding the manifestation of detectable neurodegenerative processes (25, 26). Although the precise mechanisms through which endogenous Tau facilitates neuronal deficits are still under investigation, a recently suggested pathway involves enhanced Tau-mediated postsynaptic targeting of Fyn (24); the latter is known to selectively modulate the function of GluN2B-containing NMDARs by phosphorylation of the GluN2B at its Y1472 epitope, an event that stabilizes GluN2B at the postsynaptic density, thus linking NMDARs to downstream excitotoxic cascades (24, 30). In addition to adding support for the view that stress and AD share common neurobiological substrates (31), the results presented here suggest a plausible Tau-dependent mechanism (Fig. 5) through which chronic stress

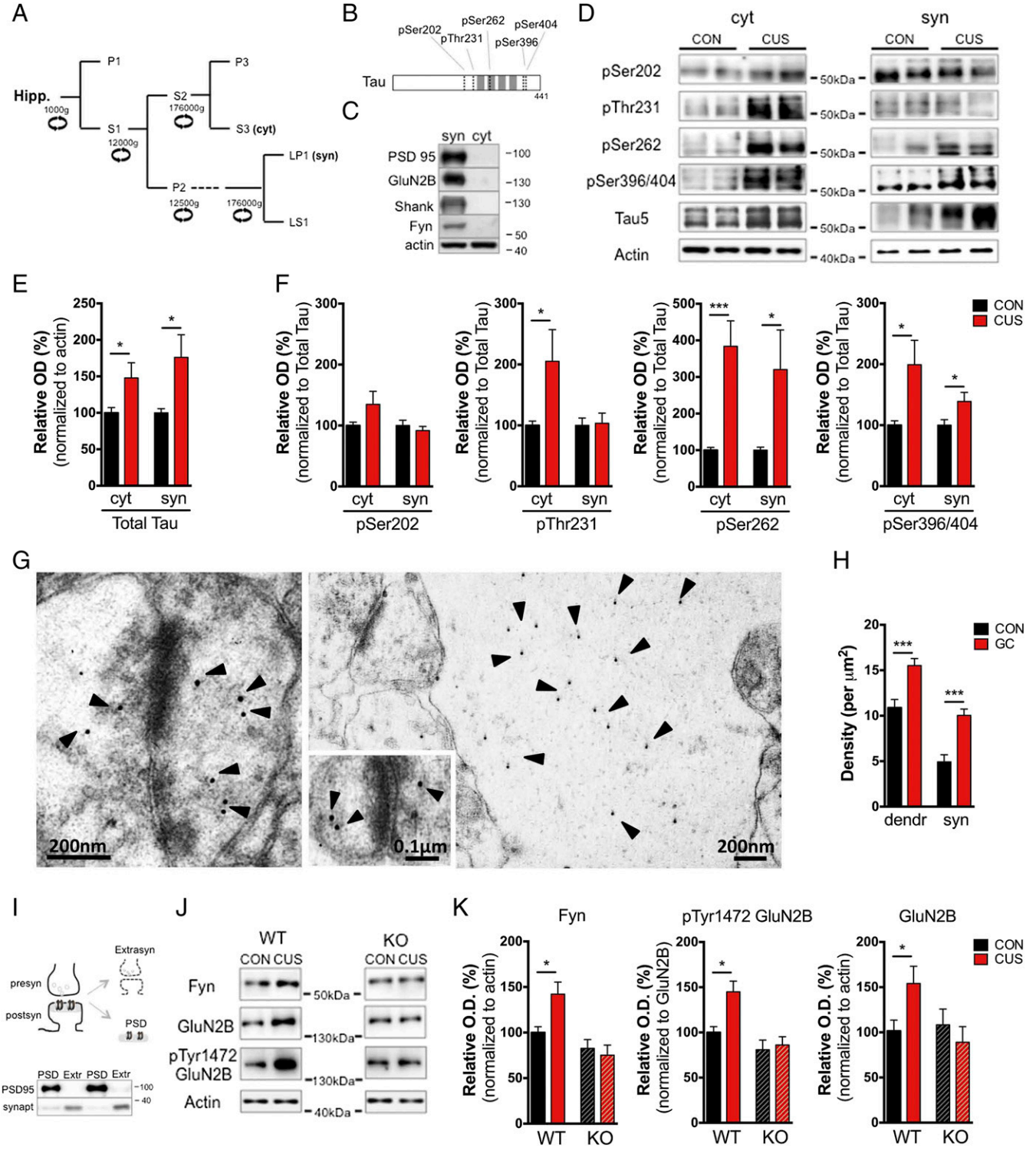

Fig. 4. Tau accumulation and missorting in the synaptic compartment of mice exposed to chronic stress. (*A*) Schematic showing the subcellular fractionation protocol used to prepare synaptosomal (LP1) and cytosolic (S3) fractions (*SI Appendix*) and (*B*) the different Tau phospho-epitopes monitored in this study. (*C*) Immunoblots showing synaptic proteins (e.g., PSD-95) and receptor (e.g., GluN2B) detected in synaptosomal, but not in cytosolic, preparations. (*D*–*F*) Exposure to CUS increased the cytosolic levels of total Tau and pThr231-, pSer262-, and pSer396/404-Tau isoforms in the hippocampi of WT mice. In addition, CUS boosted the overall levels of Tau, as well as pSer262 and pSer396/404-Tau in the synaptosomal fractions. (*G* and *H*) Transmission electron micrographs of immunogold-stained Tau in the hippocampus, showing that glucocorticoid (GC) treatment increases the amount of Tau in both dendritic and synaptic compartments. (*I*) Schematic of method used to isolate postsynaptic density (PSD) and extrasynaptic (Extra) fractions from hippocampal tissue and immunodetection of PSD95 and synaptophysin in the PSD and extrasynaptic fractions, respectively. (*J* and *K*) CUS increases Fyn protein levels in the PSD, as well as levels of total and pY1472-GluN2B in the PSD of WT, but not Tau-KO, animals. All numeric data represent mean ± SEM (*$P < 0.05$; ***$P < 0.001$).

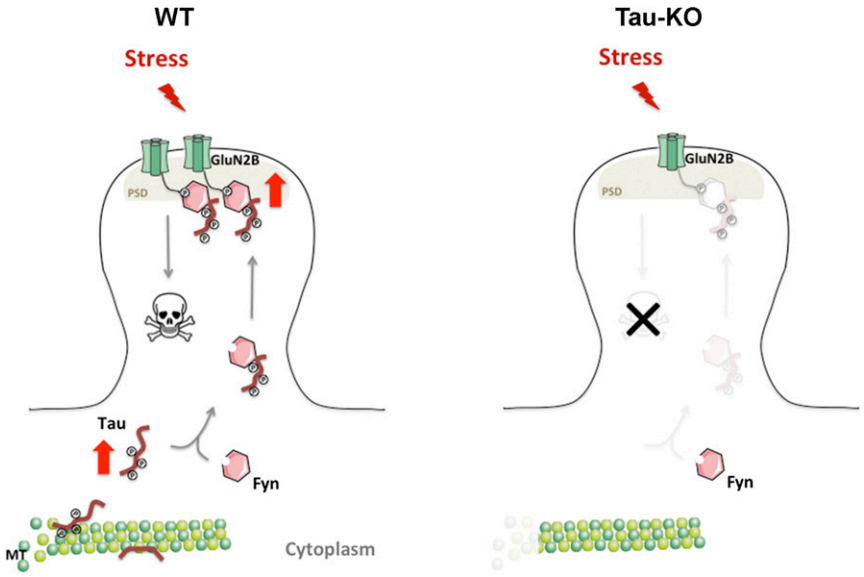

Fig. 5. Working model of how Tau plays a central role in the cellular processes underpinning the adverse effects of stress on hippocampal function. The model proposes that chronic stress leads to the hyperphosphorylation of specific phospho-Tau isotopes, which results in (*i*) dissociation of Tau from microtubules (MT), (*ii*) cytoplasmic accumulation of Tau, and (*iii*) missorting of Tau in dendritic spines. The latter targets the Src kinase Fyn to the postsynaptic density (PSD; gray box) where it phosphorylates the Y1472 epitope of the NMDA receptor subunit GluN2B, thereby increasing the stability of NMDA receptors within the PSD and coupling them to downstream excitotoxic cascades (24). These synaptic effects of stress depend critically on mediation by Tau, and the absence of Tau protects against stress-induced brain pathology.

initiates a signaling cascade that culminates in neuronal damage. Interestingly, the same mechanism was previously proposed to operate in other neuropathological conditions such as stroke and AD (24, 39). Note that NMDARs are also shown to be involved in stress-driven neurotoxicity (40) as blockade of NMDARs, but not AMPA receptors (AMPARs), attenuates the neuroremodeling actions of stress (41, 42).

The current study reveals the neuroprotective role of Tau reduction against the establishment of stress-driven hippocampal pathology. This observation is in line with other approaches using Tau-lowering strategies to tackle neuropathologies with diverse etiology (1, 3, 24). Interestingly, in line with previous reports (14, 16, 43 but also see ref. 44), the absence of Tau does not impact on the behavioral, neurostructural, or endocrine profile of adult animals under normal conditions, does not interfere with the endocrine response to stress, and thus does not pose a threat to the organism's survival. Our findings highlight Tau protein and its synaptic missorting as an essential mediator of the deleterious effects of stress on hippocampal structure and function, suggesting Tau as a key regulator of neuronal plasticity. Indeed, previous studies have shown that Tau hyperphosphorylation and neuronal/synaptic atrophy is also triggered by different intrinsic and extrinsic conditions such as acute stress (45), hypothermia (46), hypometabolism (47), and hibernation (48) in a reversible way. However, repeated/prolonged exposure to stress is known to result in sustained Tau hyperphosphorylation as well as insoluble neurodamaging Tau aggregates (11, 49, 50); additionally, reversibility of stress-induced neuronal atrophy is lost in the aged brain (51). Thus, future studies are necessary to clarify the mechanistic role of Tau in the stress-recovery process as well as to identify the potential threshold/"point of no return" between Tau-related neuroplasticity and neuropathology under stressful conditions. Based on the Tau involvement in different and interconnected behavioral domains affected by stress, and the emerging view that chronic stress shifts the overall brain connectome involving both hippocampal and frontostriatal "disconnection and reconnection" (7, 52), future work should further examine the impact of Tau on the overall stressed brain neuromatrix, monitoring the suggested switch between circuitries along the transition from acute stress condition to chronic stress brain construct (53).

Materials and Methods

Animals and Treatments. WT and Tau-KO male mice (C57BL/6J background), aged 4–6 mo, were used in this study (16); mice were group-housed (five animals per cage) with ad libitum access to food and water under standard environmental conditions (8:00 AM–8 PM light cycle; 22 °C; 55% humidity). All experiments were conducted in accordance with the Portuguese national authority for animal experimentation, Direcção Geral de Veterinária (ID: DGV9457), and Directive 2010/63/EU of the European Parliament and Council. Animals from each genotype were either (*i*) exposed to a CUS paradigm during the daily period of light or (*ii*) left undisturbed in their home cages (control, or CON). The CUS paradigm consisted of exposure to either restraint, vibrating platform, overcrowding, or a hot air stream on consecutive days, for 6 wk (11, 15). To monitor the efficacy of CUS, body weights were measured weekly, and blood serum was collected at the end of the stress period and assayed for corticosterone levels (ICN Biomedical). Experiments in mice were replicated four times (10–12 mice per group for each experimental replicate). Furthermore, in another experiment, male Wister rats, aged 4–5 mo, were treated with the synthetic glucocorticoid dexamethasone (DEX) for 15 d (daily s.c. injections of 300 μg/kg dissolved in sesame oil containing 0.01% ethanol); control animals received sesame oil (five animals per group). This dose of DEX was used because DEX is hampered in brain penetration as it is a substrate of the multidrug-resistant P-glycoprotein (54, 55).

Behavioral Analysis.

Y-maze. All animals were subjected to a two-trial test to assess spatial memory using a Y-maze (33 cm × 7 cm × 15 cm). The three arms were randomly designated as start, novel, and old arm; visual cues were placed on the edges of each arm. In the first trial (10 min), animals were allowed to explore only two arms. For the second trial (5 min), mice were placed back in the start arm but had free access to all arms of the maze. Trials were captured using a video-tracking system (Viewpoint); data are expressed as percentage of distance traveled and time spent in the novel arm.

Morris water maze. The maze consisted of a white circular pool (diameter: 170 cm; depth: 50 cm), filled with tap water (23 ± 1 °C; 25 cm of depth) and was divided into quadrants by imaginary lines; the maze was placed in a dimly lit room with extrinsic clues. During testing, a transparent escape platform (14 cm in diameter; 30 cm high), invisible to the animals, was placed in the same quadrant during five consecutive days. Each test session consisted of four trials

(maximum 120 s). Trials were captured on a video-tracking system (Viewpoint). The distance that animals swam to reach the hidden platform was recorded and used to evaluate learning and memory performances (11, 56).

NOR. NOR was tested using an open arena (33 cm × 33 cm × 33 cm). After a habituation period (3 sequential days), animals were allowed to explore two identical (familiar) objects for 10 min. After 24 h, mice were returned to the arena, where one of the familiar objects was replaced with a novel one (different shape, color, and texture). All sessions were videotaped and scored manually using Kinoscope software https://sourceforge.net/projects/kinoscope/). A discrimination index was calculated using the following formula: [(Novel Object/Novel Object + Familiar Object) − Familiar Object (Novel Object + Familiar Object)] × 100.

Elevated plus maze. Animals were placed in an EPM apparatus consisting of two open arms (50.8 cm × 10.2 cm) and two closed arms (50.8 cm × 10.2 cm × 40.6 cm), elevated 72.4 cm above the floor in a dimly illuminated room. The time spent in the open arms was monitored with an infrared camera (MedPCIV, Med Associates Inc.) over a total of 5 min (56).

Forced swim test. Active and passive coping behavior was assessed using the FST (18, 25). Briefly, mice were individually placed into transparent cylinders filled with water (24 °C; depth 30 cm). A 5-min test session for each mouse was recorded and trials were manually scored using Kinoscope software (https://sourceforge.net/projects/kinoscope/). Passive coping behavior was evaluated by immobility time and latency to immobility (18).

Sucrose preference test. Sucrose preference was tested in all animals (individually housed for 48 h) before the CUS paradigm was started. They received two drinking bottles, one containing water, the other 2% (wt/vol) sucrose. At the end of the CUS paradigm, animals were again monitored for sucrose preference. Anhedonia (reduction in sucrose preference) was calculated according to the following formula: sucrose preference = sucrose intake/total intake] × 100.

Neurostructural Analysis. For 3D morphological analysis, animals (n = 5 per group) were transcardially perfused with 0.9% saline. Brains were immersed in a Golgi-Cox solution for 14 d and transferred to 30% sucrose before being cut on a vibratome (coronal sections) and further processed as previously described (15, 23). Dendritic arborization was analyzed in the dentate gyrus, CA1, and CA3 of the dorsal hippocampus. Dendritic trees of individual neurons (25–30 neurons/area/experimental group) were reconstructed at 600× (oil) magnification using a motorized microscope (BX51, Olympus). A 3D analysis of the reconstructed neurons was performed using NeuroExplorer software (Microbrightfield), which also provided dendritic lengths. 3D Sholl analysis was used to evaluate the arrangement of the dendritic tree. For that purpose, the number of dendritic intersections with concentric spheres positioned at radial intervals of 20 mm was determined using NeuroExplorer software (MBF Bioscience) as previously described (15, 23).

HPLC Analysis. Levels of monoamines (NA, DA, and 5-HT) and their metabolites [HVA (homovanillic acid), DOPAC (3,4-dihydroxyphenylacetic acid), 5-HIAA (5-hydroxyindoleacetic acid)] were measured using high-performance liquid chromatography with electrochemical detection. Dorsal hippocampi were homogenized and deproteinized (0.1 N perchloric acid solution, 7.9 mM $Na_2S_2O_5$, 1.3 mM Na_2EDTA). After centrifugation (20,000 × g, 45 min), supernatant was analyzed using a GBC LC 1150 HPLC pump (GBC Scientific Equipment) coupled with a BAS-LC4C (Bioanalytical Systems Inc.) electrochemical detector (+800 mV), as previously described (56). Reverse-phase ion pairing chromatography was used to assay monoamines and their metabolites using an Aquasil C18HPLC column (250 × 4.6 mm, 5 μm; ThermoElectron). Samples were quantified by comparison of the area under the curve against known external reference standards using a PC-compatible HPLC software package (Chromatography Station) as previously described (56). The limit of detection was 1 pg/20 μL (injection volume). Turnover rates of 5-HT and DA (5-HIAA/5-HT as well as HVA/DA and DOPAC/DA, respectively) were calculated as indices of serotonergic and dopaminergic activity, respectively. Monoamine turnover rates are more reliable indices of neurotransmission activity than absolute levels of monoamine, as they integrate synthesis, release, reuptake, and metabolism of neurotransmitters in the synapse (56).

Electrophysiological Recordings. After brain removal in ice-cold sucrose-based artificial cerebrospinal fluid solution [in mM: 2.5 KCl, 7 $MgCl_2$, 1.25 NaH_2PO_4, 110 sucrose, 26 $NaHCO_3$, 10 glucose, bubbled with carbogen gas (95% O_2, 5% CO_2)], 300-μm axial slices of dorsal hippocampus were prepared and recorded (31 °C) in standard artificial cerebrospinal fluid [in mM: 124 NaCl, 2.5 KCl, 1 $MgSO_4$, 2 $CaCl_2$, 1.25 NaH_2PO_4, 26 $NaHCO_3$, 10 glucose, bubbled with carbogen gas (95% O_2, 5% CO_2)]. Both extracellular recordings [Multiclamp 700B amplifier (Axon Instruments) and borosilicate glass pipettes with saline (3–5 MΩ)] and stimulation (bipolar tungsten electrode) were performed in the middle of the stratum radiatum of CA1. Signals were low-pass-filtered at 3 KHz and sampled at 10 KHz. The input–output relation was monitored using a STG4002 stimulus isolating unit for Shaffer collaterals stimulation [0.03 Hz (2–8 V); stimulus strength at 30–50% of the maximum slope of the field excitatory postsynaptic potential (fEPSP)]. The paired pulse ratio was assessed before LTP induction by giving two close stimuli of varying interpulse interval (25, 50, 100, and 300 ms); ratio was calculated by dividing the slope of fEPSP 2 by fEPSP 1 (baseline 0.03 Hz). LTP was elicited by delivering three 1-s-long 100-Hz burst stimuli intervaled by 15 s. Final slopes were calculated offline using the LTP software (20). All points of each individual curve were normalized to the average value of the last 10-min baseline. Averages of the slopes of the last 6-min recordings were used for comparison of the LTP curves.

Manganese Enhanced MRI Scanning. MEMRI scans were acquired on a 7 T Avance Biospec 70/30 scanner (Bruker BioSpin). For T_1 contrast, enhancement animals were injected i.p. with manganese chloride [50 mM $MnCl_2 \times 4H_2O$ (Sigma) solution in 0.9% NaCl, adjusted to pH 7.0] using a fractionated injection protocol to minimize toxic side effects (22). Eight doses of 20 mg/kg $MnCl_2$ were injected. Animals were positioned on a saddle-shaped, receive-only coil in a prone position with stereotaxtical fixation. Body temperature was controlled by a rectal thermometer (Thermalert TH-5, Physitemp Instruments) and kept at 37 °C. Additionally, the pulse was monitored with a plethysmographic pulse oxymeter (Nonin 8600V, Nonin Medical Inc.). T_1w images were acquired using a 3D gradient echo pulse sequence [echo time (TE) = 3.2 ms, repetition time (TR) = 50 ms, matrix size = 128 × 106 × 106, zero filled to 128 × 128 × 128, number of averages = 10, field of view = 16 × 16 × 18 mm, resulting in a spatial resolution of 125 × 125 × 140.6 μm^3; experimental duration 90 min]. For MRI scanning, mice were anesthetized (isoflurane 1.3–1.6 vol% in oxygen at flow rate of 1.2–1.4 L/min) and 3D T1-weighted images were acquired. Images were reconstructed in Paravision (Bruker BioSpin) and further processed in SPM8 (www.fil.ion.ucl.ac.uk/spm), including spatial normalization to an in-house template. On the basis of the anatomical brain atlas of the C57BL/6 mouse by Paxinos and Franklin (57), a bilateral hippocampal (HPC) region was defined in normalized space on the master template. HPC masks were back-transformed to match the individual's native space, and mean signal intensities were extracted. To account for possible individual differences, HPC intensity was normalized to the intensity of the masseter muscles (22).

Subcellular Fractionation and Western Blot Analysis. An established protocol was used to obtain subcellular fractions (58, 59) (Fig. 4*A*). Briefly, hippocampal tissue was homogenized [10× homogenization buffer (sucrose 9%; 5 mM DTT; 2 mM EDTA; 25 mM Tris, pH 7.4); Complete Protease Inhibitor (Roche), and Phosphatase Inhibitor Mixtures II and III (Sigma)] and centrifuged (1,000 × g). The postnuclear supernatant was subsequently centrifuged (12,500 × g) to yield crude synaptosomal and synaptosome-depleted fractions. The latter was ultracentrifuged (176,000 × g) to yield a light membrane/Golgi fraction (P3) and a cytoplasmic fraction (S3). The crude synaptosomal fraction was lysed in a hypo-osmotic solution and centrifuged (25,000 × g) to obtain the synaptosomal membrane fraction (LP1). To obtain the PSD fraction, LP1 was incubated with 1% Triton for 5–6 min before ultracentrifugation (176,000 × g); the resulting pellet contained the PSD fraction (Fig. 4*I*).

The various fractionated samples were electrophoresed and semidry-transferred onto nitrocellulose membranes (Trans-Blot Turbo Blotting System, BioRad); membranes were blocked in 5% nonfat milk in TBS-T buffer and then incubated with the following antibodies: Tau5 (1:2,000, Abcam clone TAU5), p202-Tau (1:1,000, Abcam clone EPR2402), pThr231-Tau (1:1,000 Abcam 30655), pSer262-Tau (1:1,000, Santa Cruz 101813), PHF1 (1:2,000, recognizes p396/404-Tau; kind gift from Peter Davies), GluN2B (1:1,000, Abcam 65783), pY1472-GluN2B (1:1,000, Millipore AB5403), Fyn (1:500, Santa Cruz sc-434), PSD-95 (1:10000, NeuroMab 75028), synaptophysin (1:1,000 NeuroMab Clone 7.2), and actin (1:2,000, abcam 8226). After incubation with appropriate secondary antibody, antigens were revealed by ECL (Clarity, Bio-Rad), and signal quantification was achieved using a ChemiDoc instrument and and ImageLab software from Bio-Rad. All values were normalized and expressed as a percentage of control values.

Electron Microscopy. Hippocampi were fixed in 4% PFA and postfixed in 4% PFA/0.8% glutaraldehyde in 0.1 M of phosphate buffer (pH 7.4) for 1 h. The CA1 areas were dissected from vibratome-cut axial sections of the dorsal hippocampus and embedded in Epon resin. Ultrathin sections (500 Å) were placed on

nickel grids: Following antigen retrieval (boiling in citrate buffer for 30 min and a 5% BSA treatment for 30 min), sections were stained for Tau, using an immunogold technique. Briefly, specimens were incubated overnight with Tau5 antibody (1:30, Abcam; clone TAU5), followed by appropriate gold-labeled secondary antibody (1:15; Abcam; goat 15 nm gold). Before inspection with a JEOL JEM-1400 transmission electron microscope, sections were counterstained with sequential incubation with uranyl acetate and lead citrate. Images were obtained using a Orious Sc1000 digital camera. Fifty nonoverlapping TEM (30,000×) images of ultrathin sections per treatment group were analyzed by an experimenter blind to the in vivo treatments.

Statistical Analysis. Data were analyzed using two-way ANOVA analysis before application of post hoc comparisons (SPSS Inc. and GraphPad Software Inc.); two-way repeated measures ANOVA was used to analyze the MWM data. Differences were considered statistically significant when $P < 0.05$.

ACKNOWLEDGMENTS. We thank Dr. Peter Davies (Albert Einstein College) for the PHF1 antibody. This work was funded by Portuguese Foundation for Science & Technology (FCT) Grants PTDC/SAU-NMC/113934/2009 (to I.S.); the European Union FP7 Project SwitchBox (N.S. and O.F.X.A.); the Portuguese North Regional Operational Program (ON.2–O Novo Norte) under the National Strategic Reference Framework (QREN) through the European Regional Development Fund (FEDER); and the Education and Lifelong Learning, Supporting Postdoctoral Researchers and Large Scale Cooperative Project, cofinanced by the European Social Fund and the Greek General Secretariat for Research and Technology. J.V.-S. is a recipient of a PhD fellowship (PD/BD/105938/2014) of the University of Minho MD/PhD Program funded by the FCT.

1. Roberson ED, et al. (2007) Reducing endogenous tau ameliorates amyloid beta-induced deficits in an Alzheimer's disease mouse model. *Science* 316(5825):750–754.
2. DeVos SL, et al. (2013) Antisense reduction of tau in adult mice protects against seizures. *J Neurosci* 33(31):12887–12897.
3. Gheyara AL, et al. (2014) Tau reduction prevents disease in a mouse model of Dravet syndrome. *Ann Neurol* 76(3):443–456.
4. McEwen BS (1999) Stress and hippocampal plasticity. *Annu Rev Neurosci* 22:105–122.
5. Bessa JM, et al. (2009) A trans-dimensional approach to the behavioral aspects of depression. *Front Behav Neurosci* 3:1.
6. de Kloet ER, Joëls M, Holsboer F (2005) Stress and the brain: From adaptation to disease. *Nat Rev Neurosci* 6(6):463–475.
7. Sousa N, Almeida OF (2012) Disconnection and reconnection: The morphological basis of (mal)adaptation to stress. *Trends Neurosci* 35(12):742–751.
8. Lupien SJ, McEwen BS, Gunnar MR, Heim C (2009) Effects of stress throughout the lifespan on the brain, behaviour and cognition. *Nat Rev Neurosci* 10(6):434–445.
9. Catania C, et al. (2009) The amyloidogenic potential and behavioral correlates of stress. *Mol Psychiatry* 14(1):95–105.
10. Green KN, Billings LM, Roozendaal B, McGaugh JL, LaFerla FM (2006) Glucocorticoids increase amyloid-beta and tau pathology in a mouse model of Alzheimer's disease. *J Neurosci* 26(35):9047–9056.
11. Sotiropoulos I, et al. (2011) Stress acts cumulatively to precipitate Alzheimer's disease-like tau pathology and cognitive deficits. *J Neurosci* 31(21):7840–7847.
12. Stein-Behrens B, Mattson MP, Chang I, Yeh M, Sapolsky R (1994) Stress exacerbates neuron loss and cytoskeletal pathology in the hippocampus. *J Neurosci* 14(9):5373–5380.
13. Elliott EM, et al. (1993) Corticosterone exacerbates kainate-induced alterations in hippocampal tau immunoreactivity and spectrin proteolysis in vivo. *J Neurochem* 61(1):57–67.
14. Morris M, Maeda S, Vossel K, Mucke L (2011) The many faces of tau. *Neuron* 70(3):410–426.
15. Cerqueira JJ, Mailliet F, Almeida OF, Jay TM, Sousa N (2007) The prefrontal cortex as a key target of the maladaptive response to stress. *J Neurosci* 27(11):2781–2787.
16. Dawson HN, et al. (2001) Inhibition of neuronal maturation in primary hippocampal neurons from tau deficient mice. *J Cell Sci* 114(Pt 6):1179–1187.
17. Pinto V, et al. (2015) Differential impact of chronic stress along the hippocampal dorsal-ventral axis. *Brain Struct Funct* 220(2):1205–1212.
18. Molendijk ML, de Kloet ER (2015) Immobility in the forced swim test is adaptive and does not reflect depression. *Psychoneuroendocrinology* 62:389–391.
19. Campeau S, Liberzon I, Morilak D, Ressler K (2011) Stress modulation of cognitive and affective processes. *Stress* 14(5):503–519.
20. Anderson WW, Collingridge GL (2007) Capabilities of the WinLTP data acquisition program extending beyond basic LTP experimental functions. *J Neurosci Methods* 162(1-2):346–356.
21. Yu X, Wadghiri YZ, Sanes DH, Turnbull DH (2005) In vivo auditory brain mapping in mice with Mn-enhanced MRI. *Nat Neurosci* 8(7):961–968.
22. Grünecker B, et al. (2010) Fractionated manganese injections: Effects on MRI contrast enhancement and physiological measures in C57BL/6 mice. *NMR Biomed* 23(8):913–921.
23. Bessa JM, et al. (2009) The mood-improving actions of antidepressants do not depend on neurogenesis but are associated with neuronal remodeling. *Mol Psychiatry* 14(8): 764–773, 739.
24. Ittner LM, et al. (2010) Dendritic function of tau mediates amyloid-beta toxicity in Alzheimer's disease mouse models. *Cell* 142(3):387–397.
25. Hoover BR, et al. (2010) Tau mislocalization to dendritic spines mediates synaptic dysfunction independently of neurodegeneration. *Neuron* 68(6):1067–1081.
26. Kimura T, et al. (2007) Hyperphosphorylated tau in parahippocampal cortex impairs place learning in aged mice expressing wild-type human tau. *EMBO J* 26(24):5143–5152.
27. Tai HC, et al. (2012) The synaptic accumulation of hyperphosphorylated tau oligomers in Alzheimer disease is associated with dysfunction of the ubiquitin-proteasome system. *Am J Pathol* 181(4):1426–1435.
28. Zempel H, Thies E, Mandelkow E, Mandelkow EM (2010) Abeta oligomers cause localized Ca(2+) elevation, missorting of endogenous Tau into dendrites, Tau phosphorylation, and destruction of microtubules and spines. *J Neurosci* 30(36):11938–11950.
29. Lee G, Newman ST, Gard DL, Band H, Panchamoorthy G (1998) Tau interacts with src-family non-receptor tyrosine kinases. *J Cell Sci* 111(Pt 21):3167–3177.
30. Salter MW, Kalia LV (2004) Src kinases: A hub for NMDA receptor regulation. *Nat Rev Neurosci* 5(4):317–328.
31. Sotiropoulos I, et al. (2008) Glucocorticoids trigger Alzheimer disease-like pathobiochemistry in rat neuronal cells expressing human tau. *J Neurochem* 107(2):385–397.
32. Lauckner J, Frey P, Geula C (2003) Comparative distribution of tau phosphorylated at Ser262 in pre-tangles and tangles. *Neurobiol Aging* 24(6):767–776.
33. Hall GF, Chu B, Lee G, Yao J (2000) Human tau filaments induce microtubule and synapse loss in an in vivo model of neurofibrillary degenerative disease. *J Cell Sci* 113(Pt 8):1373–1387.
34. Sengupta A, et al. (1998) Phosphorylation of tau at both Thr 231 and Ser 262 is required for maximal inhibition of its binding to microtubules. *Arch Biochem Biophys* 357(2):299–309.
35. Mairet-Coello G, et al. (2013) The CAMKK2-AMPK kinase pathway mediates the synaptotoxic effects of Aβ oligomers through Tau phosphorylation. *Neuron* 78(1):94–108.
36. Merino-Serrais P, et al. (2013) The influence of phospho-τ on dendritic spines of cortical pyramidal neurons in patients with Alzheimer's disease. *Brain* 136(Pt 6): 1913–1928.
37. Tsushima H, et al. (2015) HDAC6 and RhoA are novel players in Abeta-driven disruption of neuronal polarity. *Nat Commun* 6:7781.
38. Wilson RS, et al. (2003) Proneness to psychological distress is associated with risk of Alzheimer's disease. *Neurology* 61(11):1479–1485.
39. Aarts M, et al. (2002) Treatment of ischemic brain damage by perturbing NMDA receptor-PSD-95 protein interactions. *Science* 298(5594):846–850.
40. Yang CH, Huang CC, Hsu KS (2005) Behavioral stress enhances hippocampal CA1 long-term depression through the blockade of the glutamate uptake. *J Neurosci* 25(17): 4288–4293.
41. Magariños AM, McEwen BS (1995) Stress-induced atrophy of apical dendrites of hippocampal CA3c neurons: Comparison of stressors. *Neuroscience* 69(1):83–88.
42. Magariños AM, McEwen BS (1995) Stress-induced atrophy of apical dendrites of hippocampal CA3c neurons: Involvement of glucocorticoid secretion and excitatory amino acid receptors. *Neuroscience* 69(1):89–98.
43. Lopes S, et al. (2016) Absence of Tau triggers age-dependent sciatic nerve morphofunctional deficits and motor impairment. *Aging Cell* 15(2):208–216.
44. Ahmed T, et al. (2014) Cognition and hippocampal synaptic plasticity in mice with a homozygous tau deletion. *Neurobiol Aging* 35(11):2474–2478.
45. Rissman RA, Lee KF, Vale W, Sawchenko PE (2007) Corticotropin-releasing factor receptors differentially regulate stress-induced tau phosphorylation. *J Neurosci* 27(24): 6552–6562.
46. Planel E, et al. (2004) Alterations in glucose metabolism induce hypothermia leading to tau hyperphosphorylation through differential inhibition of kinase and phosphatase activities: Implications for Alzheimer's disease. *J Neurosci* 24(10):2401–2411.
47. van der Harg JM, et al. (2014) The unfolded protein response mediates reversible tau phosphorylation induced by metabolic stress. *Cell Death Dis* 5:e1393.
48. Arendt T, et al. (2003) Reversible paired helical filament-like phosphorylation of tau is an adaptive process associated with neuronal plasticity in hibernating animals. *J Neurosci* 23(18):6972–6981.
49. Rissman RA, et al. (2012) Corticotropin-releasing factor receptor-dependent effects of repeated stress on tau phosphorylation, solubility, and aggregation. *Proc Natl Acad Sci USA* 109(16):6277–6282.
50. Sotiropoulos I, et al. (2015) Female hippocampus vulnerability to environmental stress, a precipitating factor in Tau aggregation pathology. *J Alzheimers Dis* 43(3): 763–774.
51. Bloss EB, Janssen WG, McEwen BS, Morrison JH (2010) Interactive effects of stress and aging on structural plasticity in the prefrontal cortex. *J Neurosci* 30(19):6726–6731.
52. Dias-Ferreira E, et al. (2009) Chronic stress causes frontostriatal reorganization and affects decision-making. *Science* 325(5940):621–625.
53. Sousa N (2016) The dynamics of the stress neuromatrix. *Mol Psychiatry* 21(3):302–312.
54. Meijer OC, et al. (1998) Penetration of dexamethasone into brain glucocorticoid targets is enhanced in mdr1A P-glycoprotein knockout mice. *Endocrinology* 139(4): 1789–1793.
55. Hassan AH, Patchev VK, von Rosenstiel P, Holsboer F, Almeida OF (1999) Plasticity of hippocampal corticosteroid receptors during aging in the rat. *FASEB J* 13(1):115–122.
56. Novais A, et al. (2013) Neudesin is involved in anxiety behavior: Structural and neurochemical correlates. *Front Behav Neurosci* 7:119.
57. Paxinos G, Franklin KBJ (2001) *The Mouse Brain in Stereotaxic Coordinates* (Academic, San Diego), 2nd Ed.
58. Kimura T, et al. (2013) Microtubule-associated protein tau is essential for long-term depression in the hippocampus. *Philos Trans R Soc Lond B Biol Sci* 369(1633):20130144.
59. Sahara N, Murayama M, Higuchi M, Suhara T, Takashima A (2014) Biochemical distribution of Tau protein in synaptosomal fraction of transgenic mice expressing human P301L Tau. *Front Neurol* 5:26.